PAPER Nr.: 22

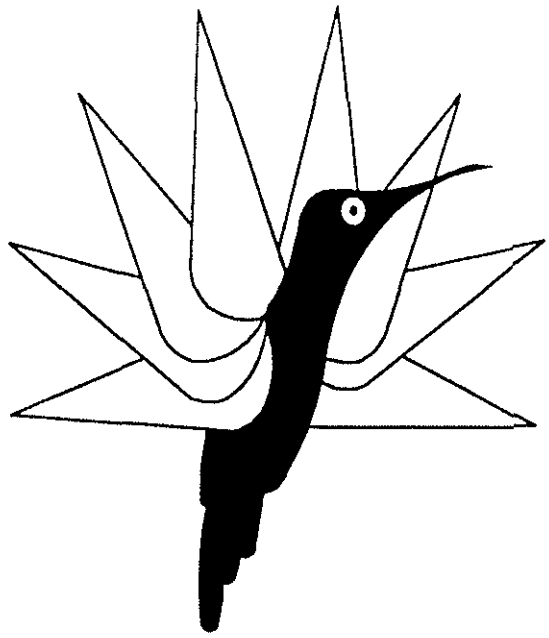

# NUMERICAL AND EXPERIMENTAL INVESTIGATIONS OF UNSTEADY FLOWS UNDER DEEP DYNAMIC STALL CONDITIONS

BY

W. GEISSLER[1], J. KOMPENHANS[1], M. RAFFEL[1],
H. VOLLMERS[1], P. WERNERT[2]

[1]Deutsche Forschungsanstalt für Luft- und Raumfahrt, e.V. (DLR), Göttingen, Germany

[2]French-German Research Institute (ISL), Saint Louis, France

TWENTIETH EUROPEAN ROTORCRAFT FORUM
OCTOBER 4 - 7, 1994 AMSTERDAM

Printed by the Technical Highschool Haarlem

# *NUMERICAL AND EXPERIMENTAL INVESTIGATIONS OF UNSTEADY FLOWS UNDER DEEP DYNAMIC STALL CONDITIONS.*

by
W.Geissler,J.Kompenhans,
M.Raffel,H.Vollmers, DLR-Göttingen
P.Wernert, ISL-St.Louis

***Abstract.***

With increasing advance ratios the retreating blades of modern helicopters encounter flow environments with severe separation and vortex shedding which are known as deep dynamic stall conditions. Recently considerable improvements have been achieved for both numerical methods and nonintrusive experimental flow diagnostic techniques to be applied to these complex highly unsteady flows. For the numerical treatment of the problem a time-accurate code based on the 2D-Navier-Stokes equations has been applied. The experimental investigation of the instantaneous flowfield was carried out by means of a Particle Image Velocimetry (PIV), in two different wind tunnel facilities: The low-speed wind tunnel of the German-French Institute, St. Louis (ISL) and the High Speed Wind Tunnel (HKG) of the DLR in Göttingen. For each wind tunnel a test set-up for oscillating models has been constructed and used throughout the measurements. Numerical and experimental data obtained under nearly the same conditions will be presented and compared in the present paper.

## *1. Introduction.*

A helicopter in high speed forward flight encounters cyclic flow separation on the retreating side of the rotordisc. This flow-phenomenon known as dynamic stall is characterized by strong vortex shedding and severe hysteresis effects of the blade loading and may lead to instabilities in interaction with the blade structure (blade stall flutter) or may be the origin of additional noise generation.

Before steps can be done towards a reduction or even avoidance of these negative effects the flows must be known in detail. The aim of the present joint effort between the DLR and the ISL was to study the mechanisms and effects of the dynamic stall phenomenon by application of numerical and experimental methods to the same flow problems. Dynamic stall occurs in incompressible flows as well as in a compressible environment. In the ISL-wind tunnel [1] only the incompressible aspects of the flow could be detected. The DLR-HKG tunnel [2] covers also the compressible low and high Mach number flow regimes.

In the past the dynamic stall problem has been tackled by a considerable number of investigators working mostly independently on either numerical or experimental methods. Recent numerical calculations were carried out on the basis of the complete flow field equations i.e. the Navier-Stokes equations, [3],[4]. Experimental work has been done in the past by measuring unsteady pressures on oscillating models equipped with in situ pressure transducers [5]. Recently field measurements by interferometry have been successfully carried out for this problem [6],[7]. In the DLR a numerical code has been developed to study the dynamic stall problem for a variety of flow parameters [8]. Special emphasis was placed on the problem to provide an adequate visual presentation of the enormous amount of unsteady flowfield data by sophisticated graphical display and analysis software and by animation of the data [9]. Video animation has proved to be very flexible and beneficial concerning the physical understanding of the complex flow fields involved.

The Particle Image Velocimetry as a nonintrusive diagnostic technique has specifically been further developed to be able to perform measurements of instantaneous flowfields in wind tunnels [10],[11]. To obtain a meaningful velocity vector field even in highly separated and

reversed flow the method of image shifting had to be implemented into the existing PIV-system by means of a high speed rotating mirror system [12].

To investigate the time-dependent flows about oscillating airfoil models special test stands have been developed in both DLR and ISL [13],[14]. Details of the investigation of the dynamic stall process at low speed flows by means of the Particle Image Velocimetry are reported in [15], comparisons of PIV-recordings with images from flow visualizations are included in [16].

## *2. The dynamic stall phenomenon.*

Comprehensive descriptions of the dynamic stall phenomenon are e.g. given in [15]. A considerable number of different parameters may influence the stall characteristics: airfoil shape, incidence variation, Mach number, Reynolds number and reduced frequency, the latter determining the time scale of the forced motion. As will be demonstrated later 3D-effects are also of major importance for the flow development: Under deep dynamic stall conditions the flow on a 2D-airfoil model will always show 3D-effects.

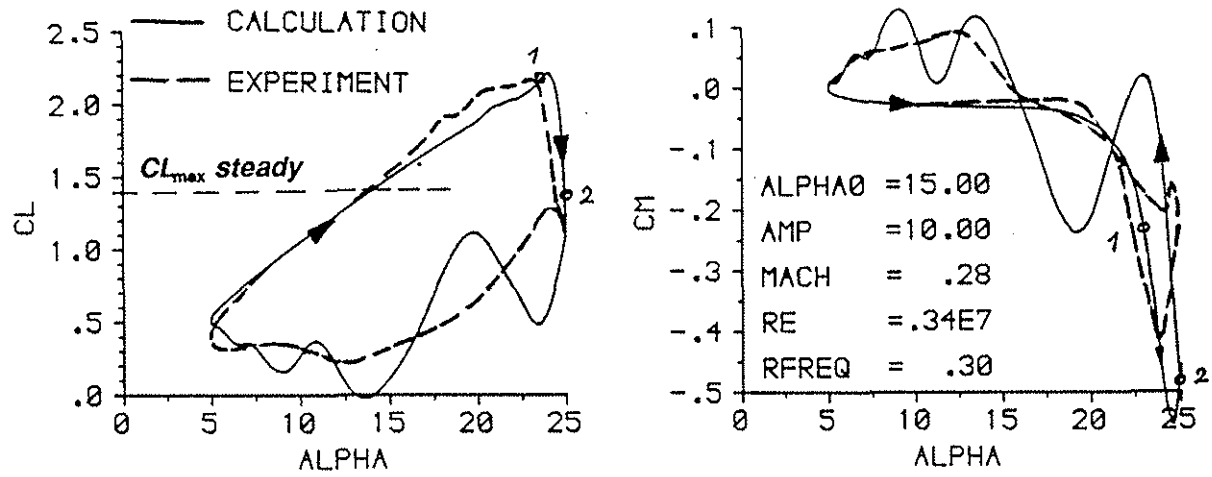


**Fig.1: Lift-and moment-loops at deep dynamic stall on NACA0012 airfoil.**

***Fig.1*** shows lift- and drag-loops of the NACA0012 airfoil during dynamic stall. Numerical results [4] are compared with experimental data [5]. The lift curve shows a considerable increase of lift compared to the steady case. It follows a steep decrease of the lift curve which takes a completely different path during the downstroke motion of the airfoil. One can observe quite good correspondence between calculation and experiment during upstroke. Larger differences occur during downstroke, which may be attributed to either 3D-effects of the flow or to smoothing due to ensemble averaging of the experimental data over a number of cycles.

Of special concern is the moment loop in Fig.1 (right): During the upstroke motion a steep decrease of the pitching moment is evident followed by a similar steep increase. This nose-down moment peak causes a strong impulsive force acting on the blade structure. The areas between the moment loops are a measure of aerodynamic damping, the direction of passing these loops determines whether positive (anti-clockwise) or negative (clockwise) damping occurs. It may happen that the overall damping is negative and a dangerous stall flutter case will appear.

These general features of dynamic stall can only be explained by detailed flowfield phenomena:

- During the fast upstroke motion of the airfoil the flow stays attached beyond the steady separation point although reversed flow occurs inside the boundary layer.
- During the high incidence range of the upstroke motion a dynamic stall vortex develops from the airfoil leading edge moving over the upper surface with about 22% of the undisturbed mainflow velocity ([18]).
- The vortex lifts off the airfoil and sheds into the wake.
- A counter-rotating vortex originates from the trailing edge and interacts with the primary vortex.
- Weaker secondary and higher order vortices start either from the leading edge (clockwise) or trailing edge (anti-clockwise) during the downstroke motion.
- Reattachment of the flow from leading to trailing edge occurs at a very late point of time within the cycle during downstroke.

It is obvious that the dynamic effects of the airfoil motion as well as the dynamics of the different vortices influence the overall forces and moments acting on the airfoil. In the present study it was possible to investigate most of the different flow structures existent during dynamic stall.

### *3. Numerical calculations.*

For the numerical investigations a time-accurate 2D-Navier-Stokes code has been developed and made applicable to the dynamic stall problem. The code is based on the "approximate factorization implicit" method of Beam and Warming [19]. The code is second order accurate in space using central differencing and first order accurate in time [4]. All present calculations are carried out on a 157x59 C-mesh which is attached to the airfoil surface and to the outer boundary. During the oscillation of the airfoil the mesh is allowed to deform. The mesh itself is numerically calculated only at the minimum and maximum incidences within the oscillatory loop. At times in between the mesh is recalculated by a simple linear interpolation procedure taking into account the two meshes in the extreme incidence positions.

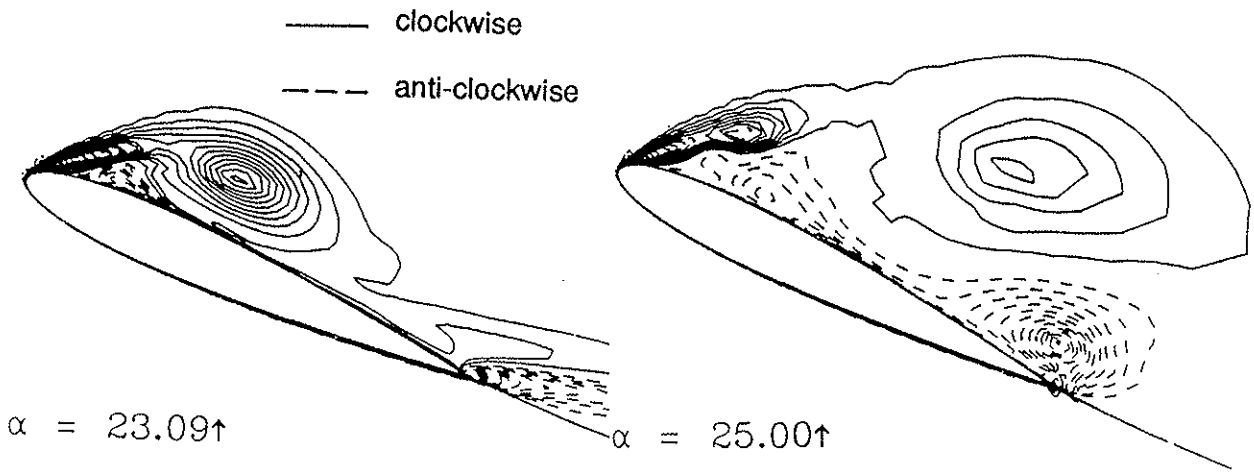


**Fig.2: Instantaneous vorticity contours on NACA0012 airfoil.**
**left: Dynamic stall vortex attached to -, right: lifted off from - the surface.**

To limit the amount of numerical damping of the finite difference method eigenvalue scaled numerical damping terms have been added [8]. For the comparison with realistic high Rey-

nolds number flows a suitable turbulence model has to be taken into account. A number of papers exist (e.g.[20]) which have investigated the effects of different turbulence models on the unsteady separated flows. Even more sophisticated k-ε-models did not do the best job. Reasonable results have even been obtained with the rather simple Baldwin/Lomax-algebraic model which has been used in the present calculations. Slight improvements specifically in separated flows were reported with the Johnson/King one-equation model. The latter approach will be implemented into the code in the near future.

***Fig.2*** shows as an example of the numerical calculation the development (left figure) and shedding (right figure) of the dynamic stall vortex. The corresponding incidences: $\alpha = 23°\uparrow$ and $\alpha = 25°$ refer to the points 1 and 2 in the lift- and moment-loops of Fig.1. The dashed vorticity contours in the right figure indicate the development of a counter-rotating vortex at the airfoil trailing edge.

### *4. Particle Image Velocimetry.*

The improvements of laser-technique in combination with the enormous increase of computer power and speed have made nonintrusive diagnostic techniques like the Laser-Doppler-Velocimetry (LDV) or the Particle Image Velocimetry (PIV) to very important tools for the investigation of complicated flows. Recently a PIV-system has been developed in DLR [10] which is able to operate successfully under the rough environmental conditions of wind tunnels. This system utilizes a two-oscillator Nd:YAG pulse laser system with a pulse energy of 2x70 mJ for illumination of an area of 20x29$cm^2$ of the flow field. The recordings are taken with a 35mm photographic camera and are analyzed by means of the Young's fringes technique.

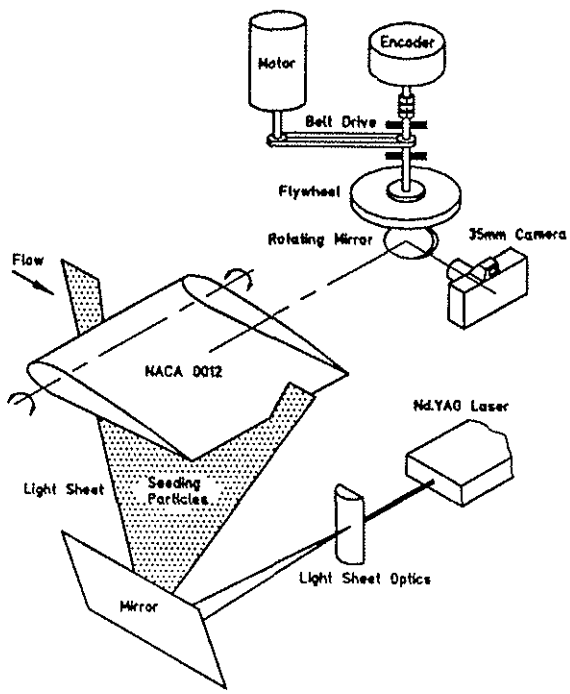


**Fig.3: Sketch of experimental set up of the PIV system in a wind tunnel.**

- Light sheet at model mid-section.
- Camera/rotating mirror-system (upper right).
- Nd:YAG Laser and Optical system for laser light sheet.

In the present studies a major improvement of the quality of the PIV data has been achieved by employing a high speed rotating mirror system for image shifting [12]. The image shifting procedure is necessary to investigate flow fields with strong reversed velocity components as e.g. in the case of the dynamic stall process. By application of image shifting the directional ambiguity of the velocity vector appearing when employing the 'dual illumination - single

frame recording' technique can be resolved. This is done by adding a constant additional displacement to the images of all tracer particles at the time of their second illumination. If this additional displacement is greater than the maximum displacement due to reverse flow, the correct velocity vector map is obtained by subtracting the additional shift from all data after evaluation of the PIV recordings.

The image shifting is achieved by a high speed rotating mirror which is mounted in front of the camera (see ***Fig.3***). The mirror is driven by a stepper motor which can establish stable rotation speeds between 1Hz and 100Hz. This leads to shift velocities from -500m/s to +500m/s respectively if a typical distance of the camera from the laser light sheet of R=0.4m is assumed.

In the present study the PIV system had to be applied to flow fields about ***oscillating*** airfoil models. For this problem it is of essential importance to be able to accurately determine the phase angle at the time of the PIV recording. Due to a limited pulse rate of the Nd:YAG laser and the performance of the winder of the camera (one picture/second) it was not possible to get a high number of recordings during only ***one*** oscillatory cycle as would be of high interest. With the technique of phase locked undersampling it was possible to obtain 6 PIV recordings within 6 seconds at exactly the same phase angle of the pitching motion with each record being taken out of a different cycle. The system was then adjusted to the next pitching angle (phase angle) of the airfoil motion in a step by step procedure. In this way the instantaneous flow fields at about 40 incidences (phase angles) have been measured.

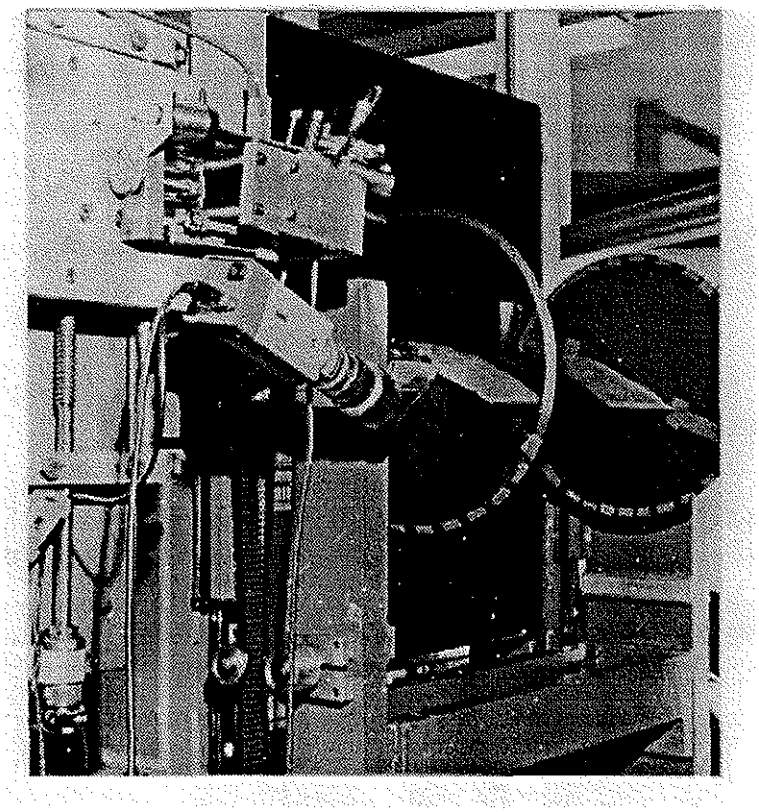

**Fig.4: Set up of the oscillating model in the open test section of the ISL-low speed tunnel.**

### *5. Wind tunnel tests.*

Two tests on oscillating airfoil models have been carried out in different wind tunnel facilities:

1. In the low speed wind tunnel of the German-French Institute St. Louis, France.

2. In the High Speed Wind Tunnel (HKG) of the DLR in Göttingen.

The ISL-tunnel [1] is of closed circuit type with an open test section. The maximum flow velocity is 35m/s ($Ma_\infty \approx 0.1$).

The HKG wind tunnel [2] is of blow down type with an open test section. The flow velocity can be selected from low Mach numbers ($Ma_\infty = 0.2$) to transonic or even supersonic Mach numbers.

***Tests in the low speed tunnel: ISL.***

***Fig.4*** shows the test setup in the open test section of the ISL wind tunnel. The rectangular test section has the dimensions: 70 cm width and 90 cm height. The length of the section is 80cm. The airfoil model with a NACA0012 airfoil section (c=20cm chordlength) was mounted between perspex endplates. The plates were fixed to the model. The driving mechanism to move the model in pitching motion about its quarter chord axis (see Fig.4) includes an automated apparatus that can be programmed by the user. Two variable speed drives, each controlling a brushless motor and a support system, are adapted to transmit the motions from the motors to the airfoil. The special feature of this driving apparatus is the possibility to operate a model in both pitching and heaving motions. Details of this system are described in [14].

In the present tests only the pitching motion has been used. To reach the conditions of deep dynamic stall, the incidence variation

$$\alpha(t) = 15° + 10° \sin(2\pi \cdot f \cdot t)$$

was chosen with a frequency of f=6.67 Hz. With a freestream velocity of 28 m/s the reduced frequency has the value

$$\omega^* = \frac{2\pi \cdot f \cdot c}{U_\infty} = 0.3 \; ; \; c = 0.2m$$

and the Reynolds number yields

$$Re = \frac{U_\infty \cdot c}{\nu} = 373000$$

which is a rather low value where transition from laminar to turbulent flow may have a considerable influence on the dynamic stall process [6].

Fig.4 shows further parts of the PIV test setup as sketched in Fig.3. The upper left part includes the camera and the rotating mirror system. Below a video camera is visible to monitor the instantaneous incidences (phase angle) of the oscillating model at the time of recording. The laser light sheet for illumination of the seeding particles was created on the upper surface of the model at its midsection. Seeding particles were added to the flow inside the settling chamber of the wind tunnel by means of a specially developed low-disturbance ejection device. Olive oil droplets of about $1\mu m$ were used as seeding material.

***Tests in the High Speed Wind Tunnel of DLR.***

***Fig.5*** shows the model with a NACA23012 airfoil section in the open test section of the DLR High Speed Tunnel. Different to the ISL tunnel the laser light sheet was created from the bottom of the test section. This arrangement made it necessary to mount the model upside down in the test section. As in the ISL experiments the model was equipped with circular endplates made from perspex. To realize high amplitude and/or high frequency pitching motions the model was made from composite material with reduced elastic deformation in both torsional and bending modes. The elastic deformation of the model was monitored by four in situ accelerometers, each two of them located close to the leading and trailing edges at the spanwise ends of the model.

Different to the electric motor driving system of the ISL tunnel the model in the High Speed Tunnel was driven by a hydraulic actuator. The right front part in Fig.5 shows the actuator/valve system. In the back upper part of Fig.5 the camera and rotating mirror systems can be seen.

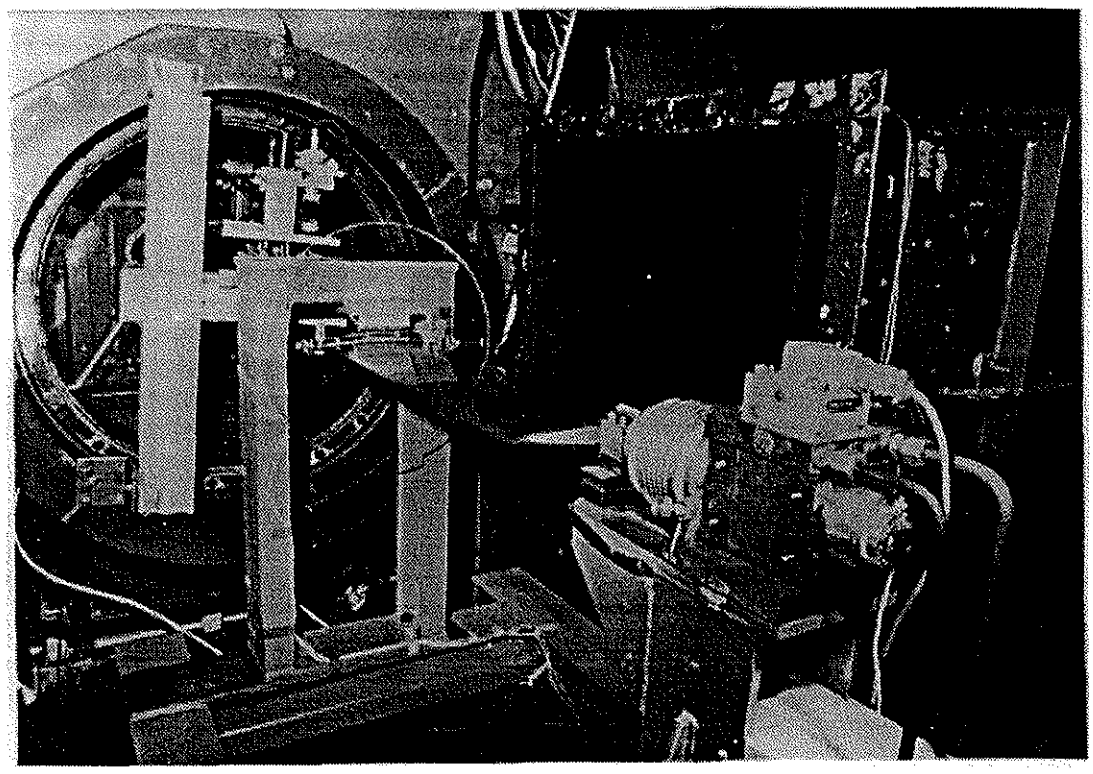

**Fig.5: Set up of the oscillating model in the open test section of the DLR-high speed tunnel.**

In addition to the accelerometers two angular position pick-ups were mounted on both spanwise ends of the model axis to monitor the incidence variation during oscillation. In addition to the PIV data aquisition system the time signals of the four accelerometers and the two angular position pick-ups as well as some additional monitoring signals were measured and further processed by means of the AMIS II [21] equipment of the DLR Institute of Aeroelasticity *). A very important point for later data reduction of the PIV recordings was the exact determination of the phase angle at recording. From this information the instantaneous incidence of the model had to be determined. This problem was solved by measuring simultaneously the trigger signal of the Pockels cell of the pulse laser and the pick up signals of the model motion with the AMIS equipment.

Experiments have been carried out with the following parameters:

| Nr. | $Ma_\infty$ | f Hz | $\omega^*$ | $\alpha_0°$ | $\alpha_1°$ | $Re \cdot 10^6$ |
|---|---|---|---|---|---|---|
| 1 | 0.2 | 10 | 0.185 | 18 | 6 | 0.91 |
| 2 | 0.3 | 10 | 0.123 | 18 | 6 | 1.36 |
| 3 | 0.3 | 6 | 0.074 | 15 | 10 | 1.36 |
| 4 | 0.75 | 29 | 0.143 | 1.5 | 1 | 3.40 |

*) The operation of the hydraulic actuator and the measurements and data reduction with the AMIS II system has been carried out by the staff of the DLR Institute of Aeroelasticity

The table shows that in order to achieve an oscillation frequency of 10Hz the amplitude had to be reduced to $\alpha_1 = 6°$. The reason for this restriction is mainly caused by the mass of the endplates which were moving with the model. For future investigations the endplates should be mounted separately from the moving model to avoid additional inertia forces.

For the dynamic stall process the dimensionless parameter $\omega^*$ is of great importance. At the ISL-measurements this parameter was considerably high $\omega^* = 0.3$. In the DLR-measurement $\omega^*$ is much lower due to the dependence of this parameter on the freestream velocity. At smaller values of $\omega^*$ however a quasi-steady flow behavior is to be expected as will be shown with the discussions of results.

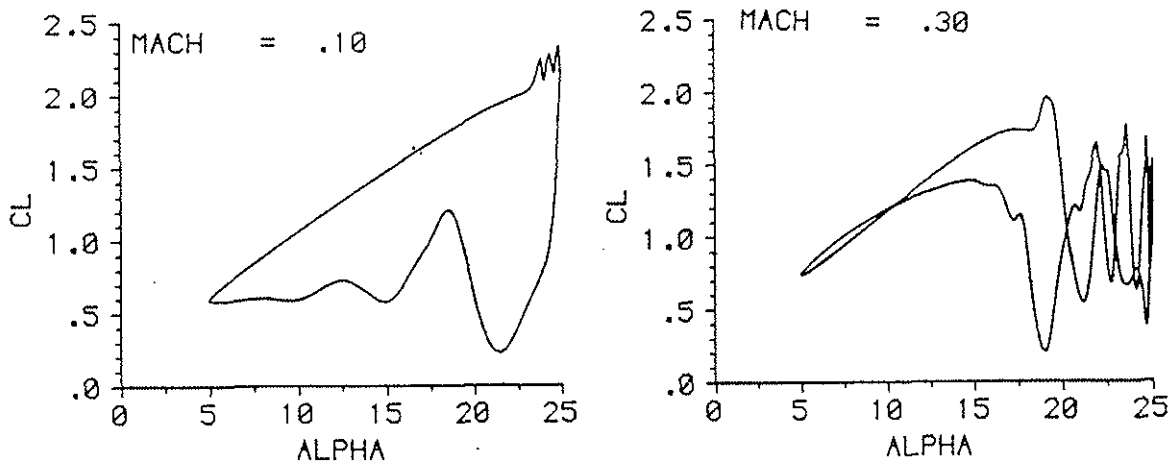


**Fig.6: Lift-distributions versus incidence:** $\alpha = 15° + 10° \sin \omega^* \cdot T$
**left:** $\omega^* = 0.3$, $Re = 3.4 \cdot 10^6$
**right:** $\omega^* = 0.074$, $Re = 1.4 \cdot 10^6$

### *6. Results.*

The dynamic stall process is influenced considerably by two parameters: Mach number and reduced frequency. The possibility to change the Mach number was the main issue for measuring in both low speed (ISL) and high speed (DLR) wind tunnels. If however, as has been mentionend before, the main flow velocity is increased, the reduced frequency is correspondingly decreased. This means that for an oscillation frequency of f=10 Hz which could be realized in both tunnels as a maximum value, the reduced frequencies are different by a factor of three. ***Fig. 6*** shows calculated distributions of lift-coefficient versus incidence for $\omega^* = 0.3$ ($M_\infty < 0.1$) and $\omega^* = 0.074$ ($Ma_\infty = 0.3$). These values refer to a frequency of 6 Hz with the incidence variation given in section 5. Several characteristic features can be detected from Fig. 6:

- In the incompressible case (Fig.6,left) the steep decrease of the lift starts at almost the maximum incidence ($\alpha = 25°$).
- In the compressible and low $\omega^*$-case (Fig.6,right) the stall occurs much earlier at about $\alpha = 18°\uparrow$.
- The post-stall behavior is quite smooth in the low Mach number case. In the higher Mach number case poststall oscillations occur which must be attributed to higher order vortex shedding in this part of the cyclic loop.

The early start of the stall process and poststall oscillations of forces and moment are typical features of a low reduced frequency behavior of the stall process.

In both ISL- and DLR- experiments it was not possible to increase the model frequency beyond 10 Hz in cases of high amplitude motions. Therefore an adjustment to the same value of $\omega^*$ for both tests could not be realized. As can be seen from the table in section 5 the amplitude of oscillation had to be reduced to $\alpha_1 = 6°$ in the case of f=10 Hz oscillation frequency. To cover the stall and poststall regimes the mean incidence of the model was then increased to $\alpha_0 = 18°$ in these cases (Test Nr.1 and 2 in table).

Finally the Reynolds number plays a very important role with respect to the transition behavior of the unsteady flow. In a low Reynolds number case transition will take place over a small laminar separation bubble during upstroke [6]. Transition in this case seems to be the reason to start the dynamic stall process at smaller incidences. In the higher Re-cases as realized in the DLR-experiments the transition from laminar to turbulent flow seems to take place without a laminar separation bubble. The start of the dynamic stall process is less effected.

All the differences in $\omega^*$, $\alpha_0$ and $\alpha_1$ as well as a different airfoil shape (NACA0012 and NACA23012) made the two tests not directly comparable. However in these experiments the main objective was to gain experience with the operation of the oscillating model test stands in combination with the complex PIV system and data reduction procedures.

In the following subsections some selected typical results from both tests and the corresponding comparisons with numerical data will be presented.

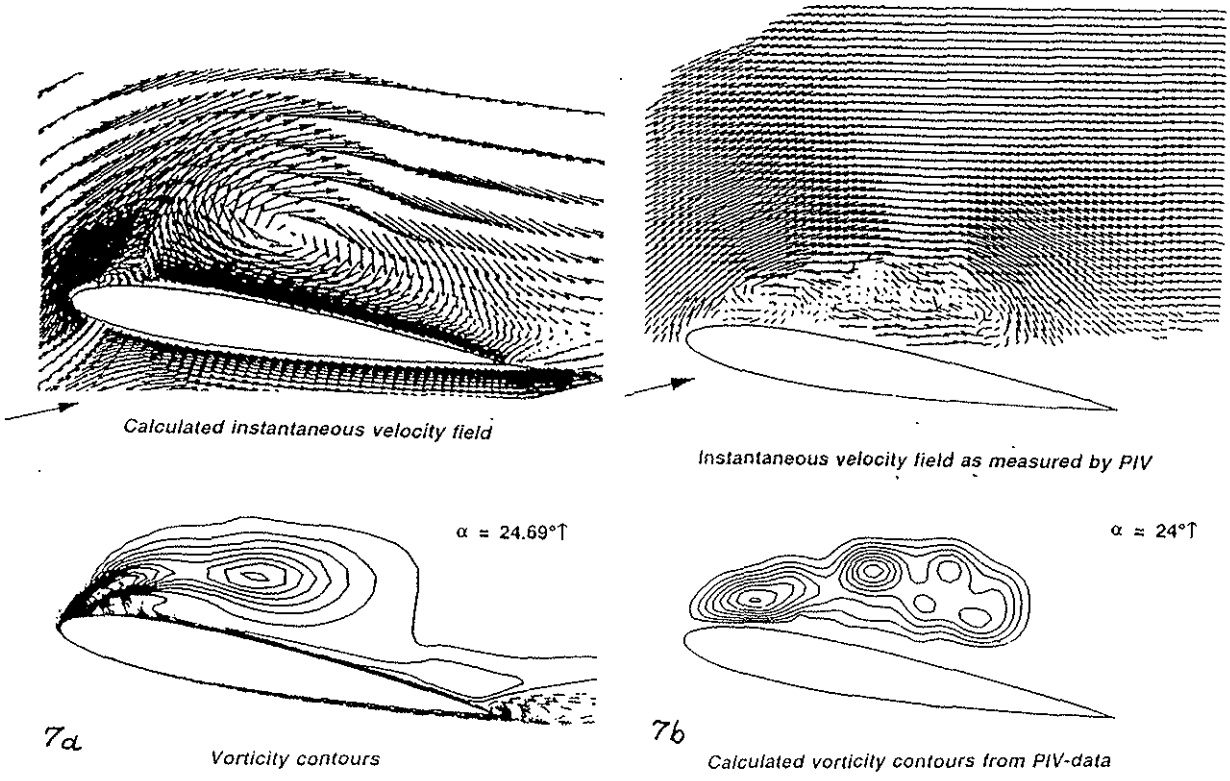


**Fig.7: Instantaneous velocity fields, vorticity contours during upstroke of NACA0012 airfoil.**
***Re*** **$= 0.4 \cdot 10^6$, $\omega^* = 0.3$**
**left (Fig.7a): Numerical Calculation.**
**right: (Fig.7b): Measured by PIV (ISL-tunnel).**

### *6a. Incompressible Flow: $Ma_\infty$ < 0.1 (ISL):*

***Figs.7*** show calculated (Fig.7a) and measured (Fig.7b) velocity vector fields during the high incidence upstroke motion of the airfoil where the dynamic stall vortex has already been

developed and started to travel along the upper surface. Below the vector fields the corresponding vorticity contours are plotted. A best fit between numerical and experimental data is achieved, if the phase angle (incidence) of the calculated result is slightly increased compared to experiment. This small phase shift may be attributed to the afore mentioned influence of a laminar separation bubble prior to the development of the vortex. The vorticity contours in Fig.7b have been calculated numerically from the experimental velocity data. In this case a smoothing procedure has been used to reduce a strong scatter of these curves. In later figures this smoothing procedure was not applied.

In the following sequences of figures the dynamic stall process will be investigated again by comparisons of numerical and experimental data. Besides of the determination of vorticity contours which are obtained by spatial differentiation of the velocity fields also the instantaneous streamlines are of considerable interest which are obtained by numerical integration of both calculated and measured velocity vector fields.

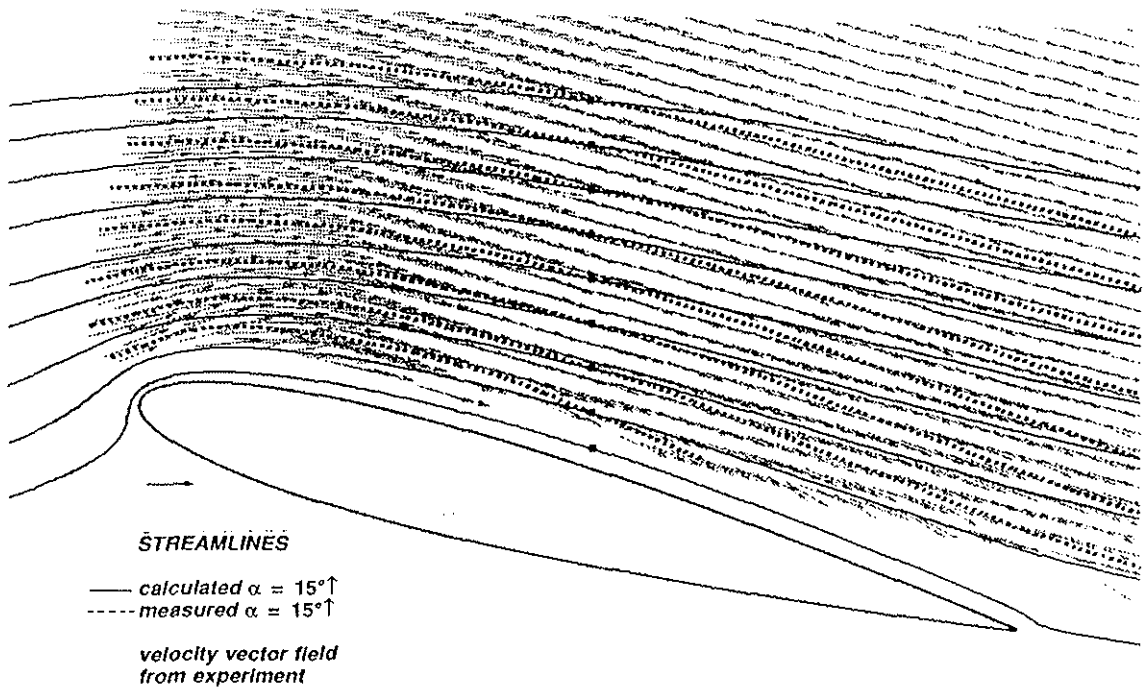


**Fig.8: Instantaneous streamlines at $\alpha = 15°\uparrow$, $Re = 0.4 \cdot 10^6$, $\omega^* = 0.3$**

### *Upstroke motion.*

***Fig.8*** shows first of all streamlines from calculations (full lines) and from the PIV-velocity field (dashed lines). The dots indicate the starting points for the streamline calculations (i.e. the same in both numerical and experimental cases). Only the experimental velocity vectors are displayed. The results of Fig.8 are plotted at $\alpha = 15°\uparrow$, i.e. at a time-instant where still no severe separation effects can be detected. The figure shows some principal deviations between calculation and experiment which must be attributed to wind tunnel effects: The bending of streamlines specifically at the outer region is considerably larger in the experimental result compared to calculations. In the latter case the assumption of free flight conditions has been approximated. The farfield boundary was assumed 10 chordlength away from the airfoil in all spatial directions. A wind tunnel correction has not been applied in the present results.

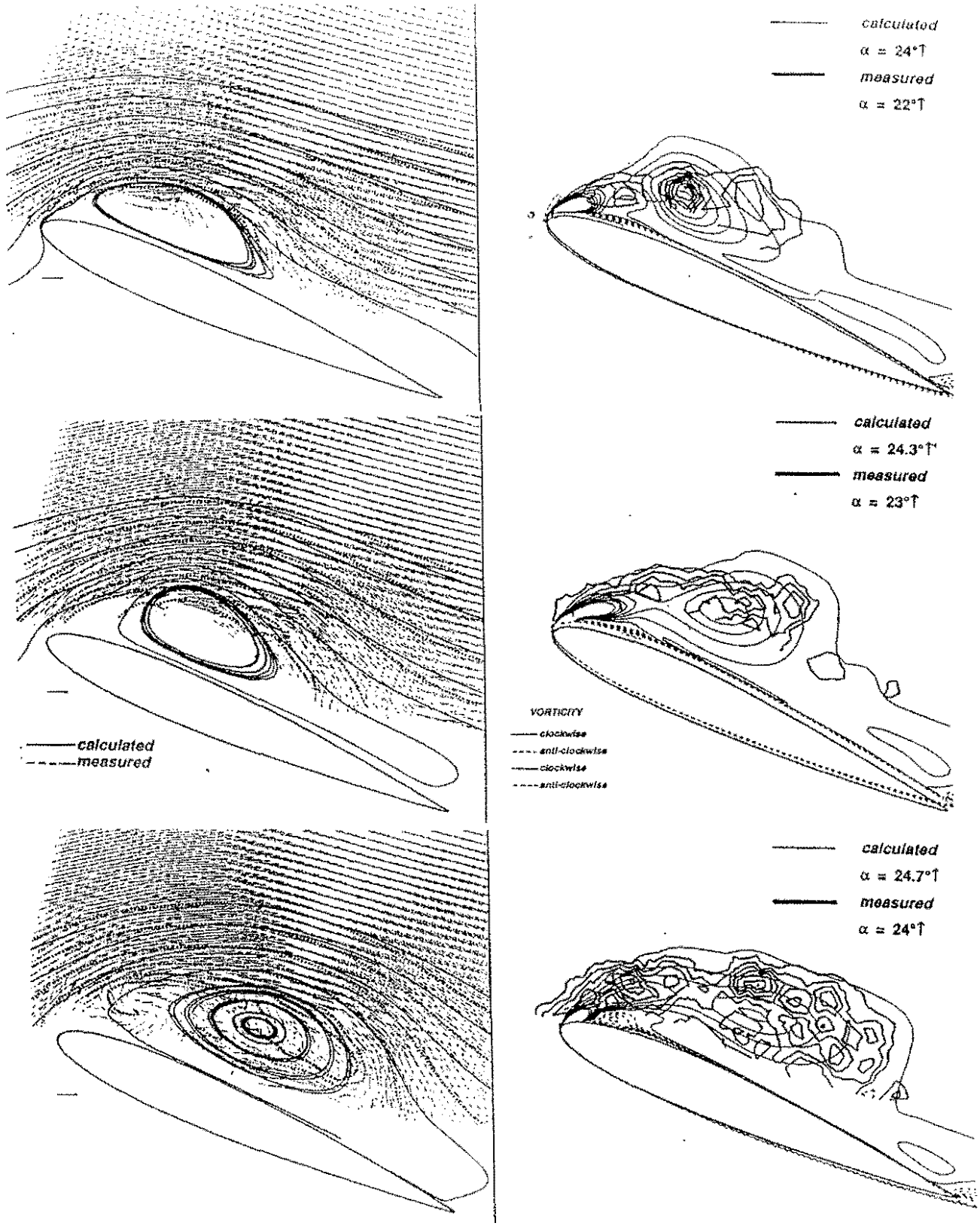


**Fig.9: Upstroke motion.**
**Streamlines (left) and vorticity contours (right) for NACA0012 airfoil in the high incidence upstroke motion: Start and movement of the dynamic stall vortex.**

$Re = 0.4 \cdot 10^6$ , $\omega^* = 0.3$

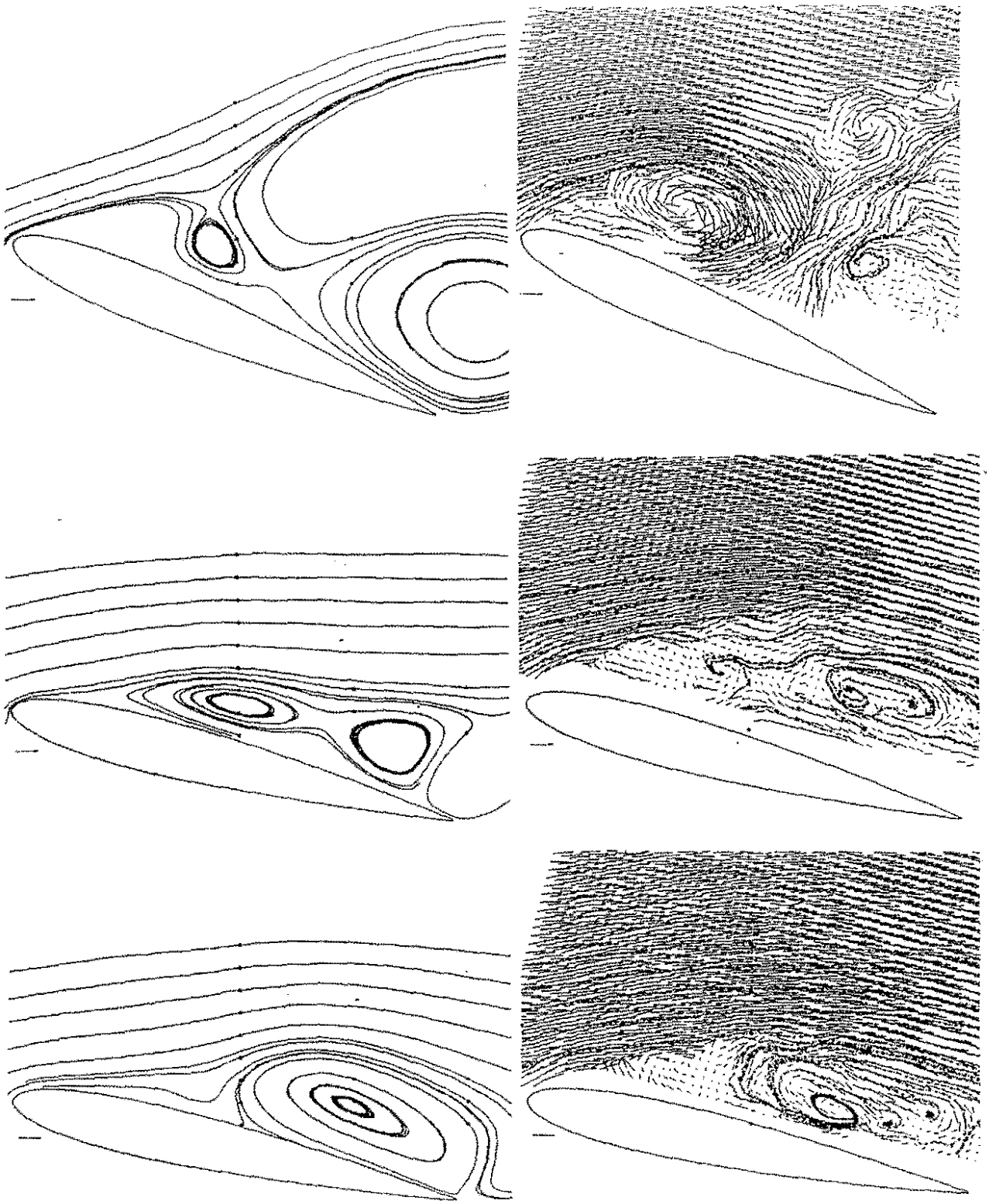

**Fig.10: Downstroke motion.**
**Calculated streamlines (left), velocity vectors and streamlines from PIV-measurements (right).**
**upper: $\alpha$ = 23°↓, middle: $\alpha$ = 15°↓, lower: $\alpha$ = 13°↓**

$Re = 0.4 \cdot 10^6$, $\omega^* = 0.3$

*Fig.9* displays a series of streamline- and vorticity contour-plots during the high incidence range of the upstroke motion. The streamline figures again include full lines from numerical calculation and dashed lines from the PIV-recordings.

The series of right hand figures includes vorticity contours. The thin lines are from numerical calculations, the thick lines are calculated from the measured velocity fields. Different to Fig.7 the vorticity contours from the measured flowfield are not smoothed. Therefore some scatter appears in these figures.

The following main features can be detected from Fig.9:

- From both streamline- and vorticity contour-plots the development of the dynamic stall vortex and its movement along the upper surface of the airfoil can be clearly seen.
- The correspondence between numerical calculations and measurements is already satisfactory.
- With increasing incidence a decreasing phase shift of events between calculation and measurement exists which may be attributed to the effect of a laminar separation bubble which shifts the start of the dynamic stall process to slightly lower incidences (phases).
- The reproducibility of these results is not exact but reasonable within this part of the cyclic loop. It was mentioned already in section 4 that a total of 6 PIV-recordings has been measured for each single phase angle allowing the investigation of reproducibility.
- In the measurements a time-stepping with $\Delta\alpha = 1°$ has been used. Due to the harmonic variation of incidence versus time this step is considerably too large. In the maximum incidence regime important information is therefore missing in the experimental data just during the time-instants of dynamic stall vortex shedding.

***Downstroke motion.***

***Fig.10*** shows some selected results during the downstroke motion of the airfoil. In this case only streamlines are displayed: The left figures show streamlines from numerical calculations. The right figures show corresponding streamlines calculated from the velocity fields of the PIV-recordings. To gain more information in the separated flow fields additional starting points for the streamline calculations were introduced at 75% and 100% chord respectively.

In the upper figure ($\alpha = 23°\downarrow$) three separated flow areas can be distinguished in both calculated and measured results. The extent of these areas is more than one chordlength out into the fluid. During downstroke the number of separated flow areas reduces to two (middle figure) and finally to one (lower figure). The extensions of these areas reduce with decreasing incidence.

Strong hysteresis effects occur between upstroke and downstroke motions: At $\alpha = 15°\uparrow$ (Fig.8) no separation effects occure. At $\alpha = 15°\downarrow$ (Fig.10,middle) flow separation is still existent. A completely undisturbed flow is finally obtained at $\alpha < 8°\downarrow$.

In contrast to the upstroke motion the flow during downstroke seems to be extremely sensitive probably due to small disturbances in the uncoming flow. The sequences in Fig.10 have been selected from different PIV-recordings (at the same phase angle) to obtain the best fit to the numerical results. Quite large deviations occure between different PIV-recordings at the same phase angle [16].

***3D-Effects.***

For the investigation of 3D-effects in the measured flow fields the divergence operator

$$div\, w = \frac{\partial u}{\partial x} + \frac{\partial v}{\partial y}$$

has been calculated from the measured velocity fields with u,v as the velocity components in x,y-directions respectively. ***Fig.11*** shows as a result contour plots of *div w* at $\alpha$ = 15°↑ (left) and $\alpha$ = 15°↓ (right) of the oscillatory motion. It has already been pointed out in Fig.8 and Fig.10 that at $\alpha$ = 15°↑ the flow is attached but at $\alpha$ = 15°↓ separated flow is still existent. The plots of *div w* in Fig.11 show only small values close to the airfoil surface for the attached flow case (left figure). At separated flow conditions (right figure) however a considerable amount of both positive and negative values of *div w* occurs, which is assumed as an indirect indicator of spanwise velocity components.

**Fig.11: Contours of *div w*, left: $\alpha$ = 15°↑, right: $\alpha$ = 15°↓**

### *6b. Compressible flow: $Ma_\infty$ = 0.3 (DLR):*

The experimental investigations in the DLR High Speed Wind Tunnel (HKG) have been carried out with the NACA 23012 airfoil model and test set up shown in Fig.5. From the large amount of data only test Nr.2 (see table on page 22-7) has been evaluated so far.

A stepping in phase angle ($\Delta\phi$ = 10°) was realized for the PIV-recordings rather than a stepping in incidence ($\Delta\alpha$ = 1°) as in the ISL measurements. Beside of these differences in airfoil shape and time stepping procedures the two tests were different in Machnumber and reduced frequency. Numerical calculations for this case have shown, that a supersonic bubble develops at the airfoil leading edge. At about $\alpha$ = 17.5°↑ this bubble disappears and at the same time the dynamic stall process starts. Before reaching the maximum incidence ( $\alpha$ = 24°) a number of higher order vortices are alternatively created and shedded from the leading edge (clockwise) and trailing edge (anti-clockwise) respectively. This vortex shedding is continued into the downstroke region. A total number of seven vortices (of each type) could be detected from the calculations. This vortex shedding has considerable effects on forces and moment: Fig.6 (right) shows the lift distribution versus incidence for a similar flow case with a number of wiggles during the high incidence motion. It has been discussed before, that the reason for this higher order vortex shedding is a rather small reduced frequency.

The question arises wether this flow behavior based on 2D-flow calculations is realistic compared to what is measured on a windtunnel model. ***Fig.12*** shows a comparison of velocity vectors during the downstroke motion of the airfoil. Fig.12 (left) shows calculated data, Fig.12 (right) displays the corresponding experimental data obtained by PIV. Although these results give only limited informations about the complex unsteady flow structures involved some common features can be clearly detected:

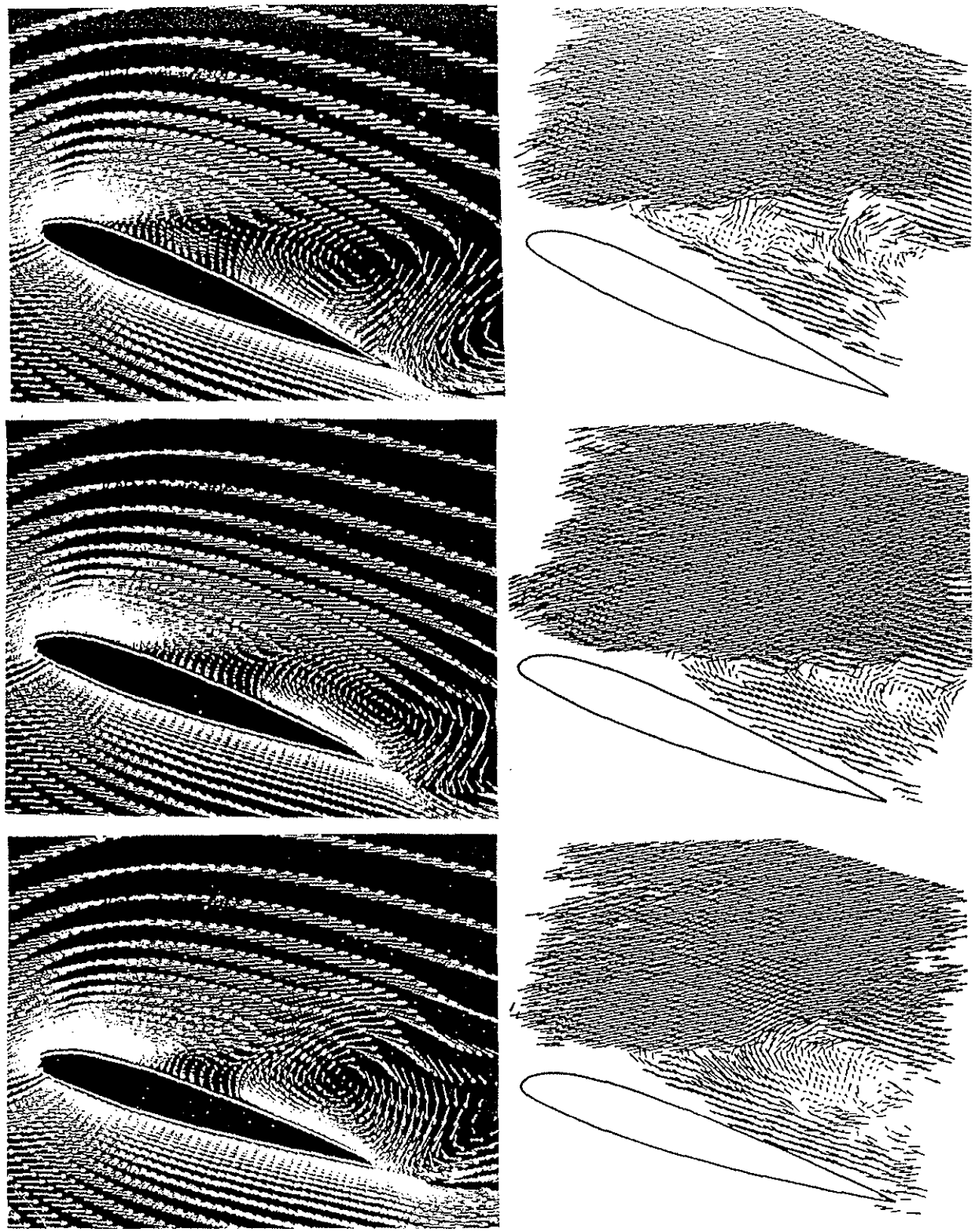

**Fig.12: Downstroke motion of NACA23012 airfoil in HKG Wind Tunnel**
**Velocity vectors, left: calculations, right: experiment**
**Upper: $\alpha$ = 23.6°↓, middle: $\alpha$ = 21.8°↓, lower: $\alpha$ = 18.4°↓**
**$\alpha = 18° + 6° \sin \omega^* T$, $Ma_\infty = 0.3$, $\omega^* = 0.123$, $Re = 1.36 \cdot 10^6$**

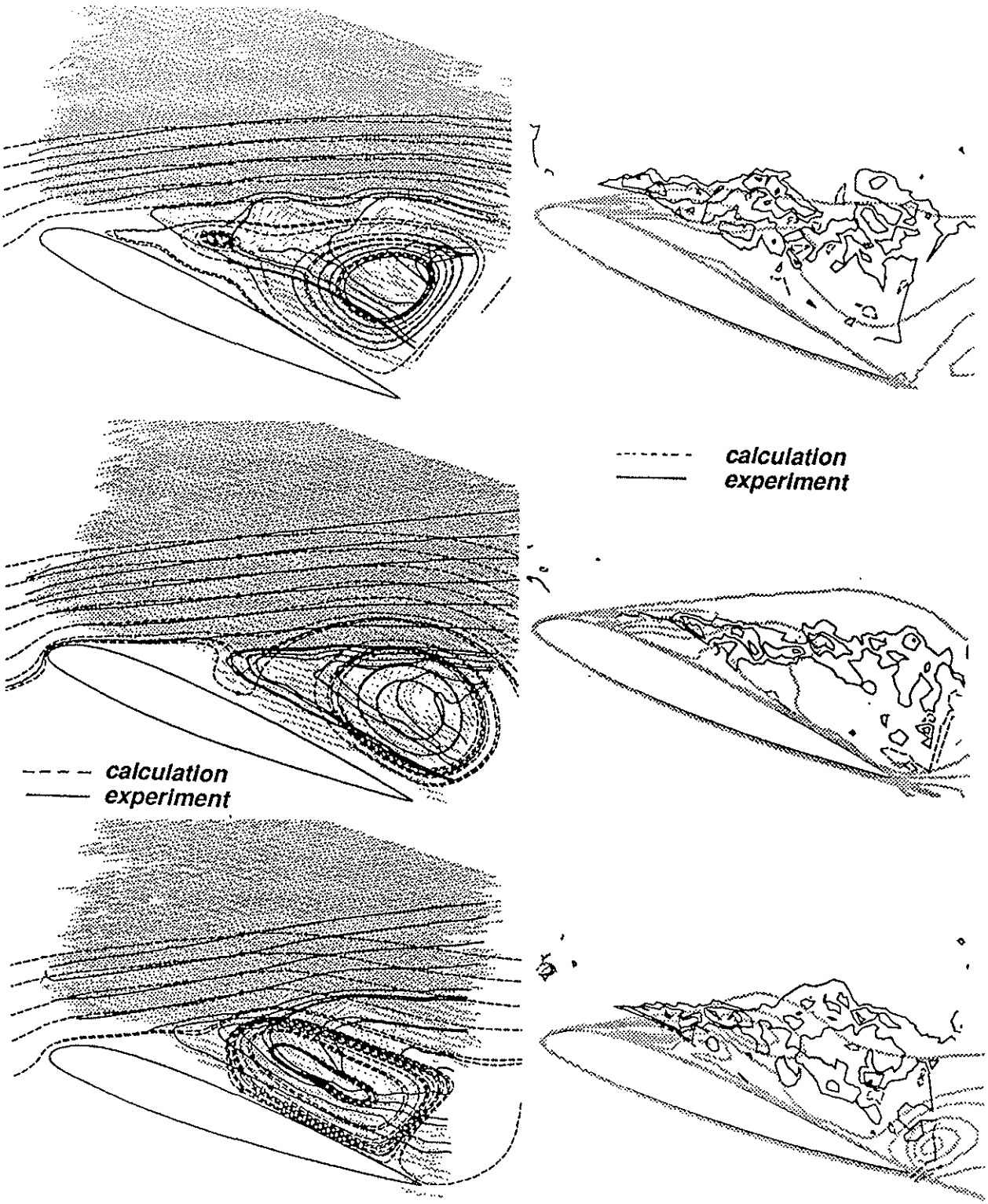


**Fig.13:** Downstroke motion of NACA23012 airfoil in HKG Wind Tunnel
Streamlines (left), vorticity contours (right)
Upper: $\alpha = 23.6°\downarrow$, middle: $\alpha = 21.8°\downarrow$, lower: $\alpha = 18.4°\downarrow$
$\alpha = 18° + 6° \sin \omega^* T$, $Ma_\infty = 0.3$, $\omega^* = 0.123$, $Re = 1.36 \cdot 10^6$

- similar velocity field structures
- corresponding vortex locations and strengths
- fluctuation of the wake, i.e. a time-dependent extension of the wake normal to the airfoil surface

***Fig.13*** finally shows streamlines (left) and vorticity contours (right) during downstroke for the same incidence variation as in Fig.12. Although calculation and experiment deviate in some parts of the figures there is on the other hand a surprisingly good correspondence in both streamline and vorticity plots. Differences similar as in the ISL data are also found in the HKG measurements: PIV recordings measured at the same phase angle but at different cycles deviate considerably specifically during the downstroke motion of the airfoil. The question how these unsteady fluctuations may affect the forces and moment acting on the model can only be answered if in addition to the velocity field measurements by PIV corresponding instantaneous pressure measurements are carried out simultaneously. In future investigations an instrumented model will therefore be used to handle these problems.

## *7. Conclusions, future activities.*

The unsteady separated flow on oscillating airfoils under deep dynamic stall conditions has been investigated by both numerical calculations and an experimental (nonintrusive) diagnostic technique: For the numerical calculations a 2D-time accurate Navier-Stokes code has been used. The experiments have been done by means of the Particle Image Velocimetry (PIV). The measurements were carried out in two different wind tunnel facilities, i.e. in the low speed tunnel of the German-French Institute St. Louis (France) and in the High Speed Wind Tunnel (HKG) of the DLR, Göttingen. In both wind tunnels special test set ups with driving mechanisms have been developed to set the 2D-models into a high amplitude pitching motion. A maximum frequency of 10 Hz could be realized in both cases.

The amount of calculated and measured data is rather large and only some few selected results have been discussed in the present paper. In general it can be stated, that numerical and experimental data show quite good correspondence during the upstroke motion of the airfoil as long as the dynamic stall vortex is developing and closely attached to the airfoil. As soon as the strong dynamic stall vortex has been shedded into the wake, the comparison of numerical and experimental data shows larger deviations. In addition the measured velocity fields obtained from different cycles of oscillation deviate considerably at the same phase angles. These deviations may be attributed to different reasons, e.g.

- influences of disturbances included in the uncoming flow
- 3D-effects at unsteady separation causing sensitive flow reactions
- errors during the experimental data reduction procedure: e.g. not exact determination of instantaneous phase angles (incidences) and airfoil locations associated with the velocity vector fields.

On the other hand also the numerical calculations have limitations due to a number of shortcomings, e.g.

- simple algebraic turbulence model
- fixed or prescribed transition (full turbulent calculations in the present case)
- 2D-calculations

These limitations in the experiments as well as in the calculations make it necessary to think about future improvements:

It would be of considerable interest to get more experimental data out of *one single cycle* of model oscillations. Here a new high speed video camera system recently developed in DLR will improve information. Another new approach of the PIV-system is directed towards determination of the third (out of plane) velocity component in the PIV recordings. It has been outlined in the present paper that 3D-effects are always existent in an unsteady separated flow even if a 2D-model is used.

The numerical code is extended to a more sophisticated type of turbulence model, i.e. the Johnson/King model. The extension of the code to 3D-calculations is also envisaged.

***Acknowledgement.***

The authors would like to acknowledge the excellent support of both DLR and ISL wind tunnel devisions and thank the AMIS II staff of the DLR Institute of Aeroelasticity for their assistance with the hydraulic- and data aquisition-systems during the HKG measurements.

***8. References.***

1. Jaeggy,B.C., Description et caracteristiques de la soufflerie subsonic de 70cmx90cm de l'ISL.
   ISL-Report N 608/82 (1982).

2. Wedemeyer,E., Der Hochgeschwindigkeitskanal der AVA.
   DFVLR-AVA-Bericht,IB 251, 77A37 (1977).

3. Ekaterinaris,J.A., Compressible Studies on Dynamic Stall.
   27th-Aerospace Sciences Meeting January,9-12,1989,Reno,Nevada
   AIAA-paper 89-0024.

4. Visbal,M.R., Effect of Compressibility on Dynamic Stall of a Pitching Airfoil.
   January,1988 AIAA-paper 88-0132.

5. McCroskey,W.J., McAllister,K.W., Carr,L.W., Pucci,S.L., An Experiment Study of Dynamic Stall on Advanced Airfoil Sections.
   NASA TM 84245,July 1982,Vol.1-3.

6. Carr,L.W., Chandrasekhara,M.S., Brock,N.J., A Quantitative Study of Unsteady Compressible Flow on an Oscillating Airfoil.
   AIAA 22nd Fluid Dynamics & Lasers Conference,June 24-26,1991, Honolulu,Hawaii.

7. Chandrasekhara,M.S., Carr,L.W., Compressibility Effects on Dynamic Stall of Oscillating Airfoils. Symposium: Aerodynamics and Aeroacustics of Rotorcraft.
   10-14 Oct.,1994,Berlin,Germany.

8. Geissler,W., Instationäres Navier-Stokes Verfahren für beschleunigt bewegte Profile.
   DLR-FB 92-03 (1992).

9. Geissler,W., Vollmers,H., Unsteady Flows on Rotor-Airfoils.
   -Analysis and Visualization of Numerical Data-
   18th European Rotorcraft Forum, 15-18 Sept.,1992,Avignon,France.

10. Kompenhans,J., Raffel,M., Vogt,A., Fischer,M., Aerodynamic Investigations in Low and High Wind Tunnels by means of Particle Image Velocimetry.
    ICIASF'93,Record,St. Louis,France,20.-23.9.1993,
    IEEE publication 93CH3199-7,pp.46.1-46.5

11. Kompenhans,J., Raffel,M., Application of PIV technique to transonic flows in a blow-down wind tunnel.
    in 'Optical Diagnostics in Fluid and Thermal Flow';S.S.Cha et al. (Eds.),Proc.SPIE 2005,pp425-436.

12. Raffel,M., PIV Messungen Instationärer Geschwindigkeitsfelder an einem schwingenden Rotorprofil.
DLR-FB 93-50 (1993).

13. Tichy,L., Transsonische Strömungen an einem schwingenden Profil und deren Einfluß auf die Flattergrenze.
DLR-FB 92-08 (1992).

14. Wernert,P., Koerber,G., Wietrich,F., A New Experimental Apperatus for the Study of Unsteady Flowfields over an Airfoil in Pitching and Heaving Motions Using Laser Doppler Anemometry.
Proc. European Forum on Wind-Tunnels and Wind-Tunnel Test Techniques. Southhampton,UK,14-17 Sept.,1992, paper 45 and ISL-Report CO 229/92.

15. Raffel,M.,Kompenhans,J.,Wernert,P.
PIV investigation of the unsteady flow velocity field above a NACA0012 airfoil pitching under deep dynamic stall conditions.
Prepared to be published in: Experiments and Fluids, June,1994.

16. Wernert,P.,Koerber,G.,Wietrich,F.,Raffel,M.,Kompenhans,J.
Experimental study of the dynamic stall process on a pitching airfoil by means of PIV measurements and laser-sheet visualizations.
Proceedings of the Seventh International Symposium on Applications of Laser Techniques to Fluid Mechanics,Lisbon,Portugal,July 11-14, 1994,paper no. 38.1.

17. McCroskey,W.J., Unsteady Airfoils.
Ann.Rev.Fluid Mech.,1982,pp 285-311.

18. Geissler,W., Numerical Investigation of Dynamic Stall on Oscillating Airfoils. Int. Forum on Aeroelasticity and Structural Dynamics 1991.
June,3-5,1991,Eurogress Center,Aachen,Germany.

19. Beam,R.M., Warming,R.F., An Implicit Finite Difference Algorithm for Hyperbolic Systems in Conservation Law Form.
J. of Comp. Physics 22,87-110,(1976), pp 87-110.

20. Srinivasan,G.R., Ekaterinaris,J.A., McCroskey,W.J., Dynamic Stall on an Oscillating Wing. Part 1: Evaluation of Turbulence Models.
AIAA 11th Applied Aerodynamics Conference, August,9-11,1993, Monterey,California.

21. Wagener,J.,Wagner,W.,Weitemeier,B.,Winter,M.,
AMIS II
Anlage zur Messung zeitveränderlicher mechanischer Größen in Windkanal Versuchen,
DLR-Nachrichten,Heft 76 (August 1994).